

Supplemental Figures

Zinc induced changes in the BDNF Met prodomain confers synaptic elimination

Jing Wang^{1*}, Agustin Anastasia^{2*}, Henrietta Bains¹, Joanna I. Giza³, David G. Clossey⁴,
Jingjing Deng⁵, Thomas A. Neubert⁵, William J. Rice⁶, Francis S. Lee³, Barbara L.
Hempstead^{4,8}, Clay Bracken^{1,8,9}

¹ Weill Cornell Medicine, Department of Biochemistry, New York, NY

² Instituto Ferreyra (INIMEC-CONICET-Universidad Nacional de Cordoba),
Córdoba, Argentina

³ City University of New, Department of Science, York, New York, NY

⁴ Weill Cornell Medicine, Department of Medicine, New York, NY

⁵ New York University School of Medicine, Skirball Institute and Department of Cell
Biology, New York, NY

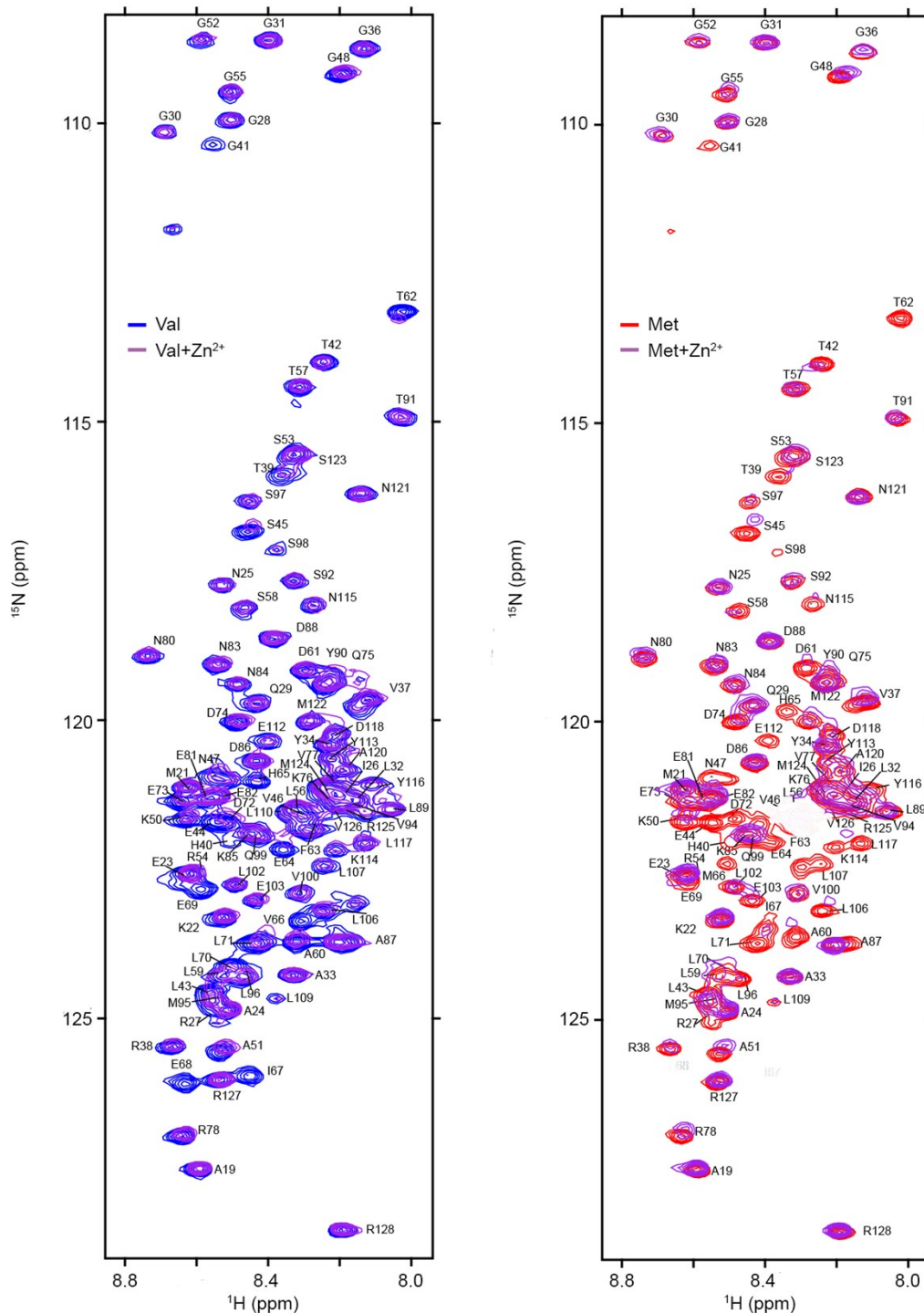
⁶ New York University School of Medicine, New York, NY

⁷ Weill Cornell Medicine, Department of Psychiatry, New York, NY

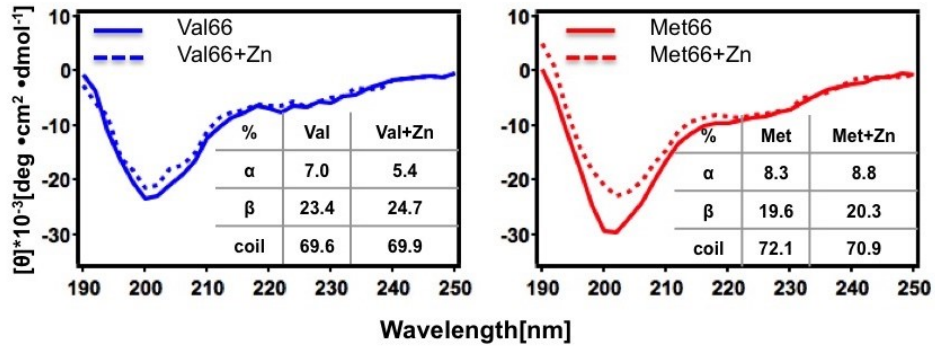
⁸ Corresponding authors

⁹ Lead Contact

* These authors contributed equally to this work.

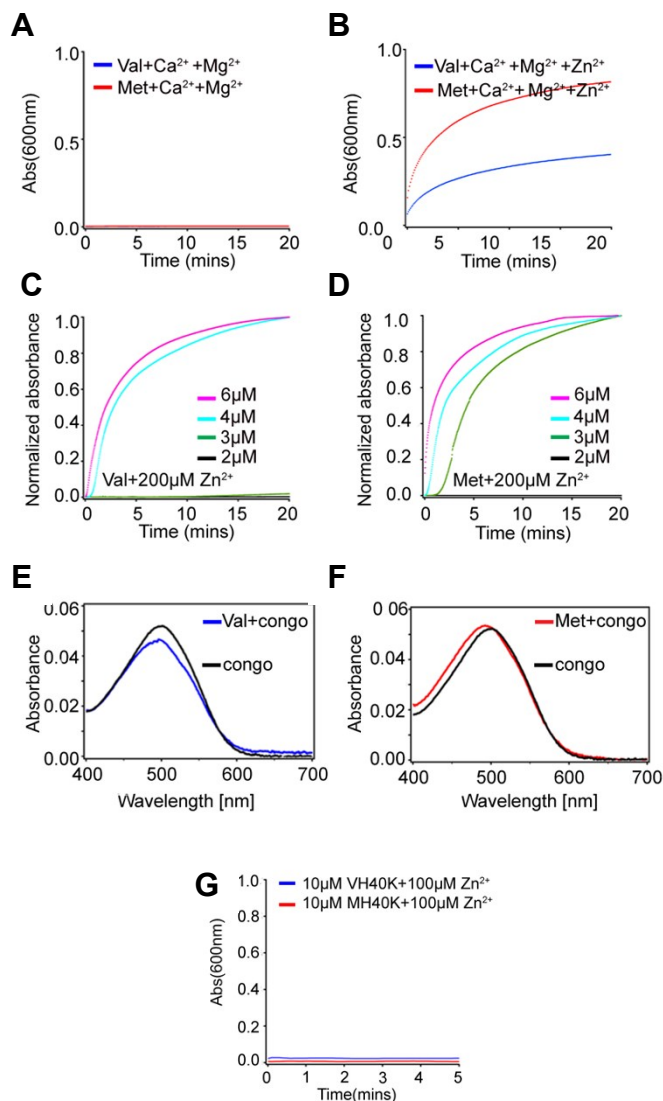


Supplemental Figure 1. Zn²⁺ Induced NMR changes. ¹H-¹⁵N HSQC NMR spectra collected using an Avance IIIHD-600 equipped with a TCI cryoprobe, data obtained at 5 °C at a ¹H field strength of 600MHz, on 8 μM prodomain for (A) Val66 (blue) and (B) Met66 (red) prodomain in the apo state and in the presence of sub-stoichiometric prodomain:zinc ratio (1:0.5) 4 μM Zn²⁺ spectra overlaid shown in purple for both Val-Zn²⁺ and Met-Zn²⁺.



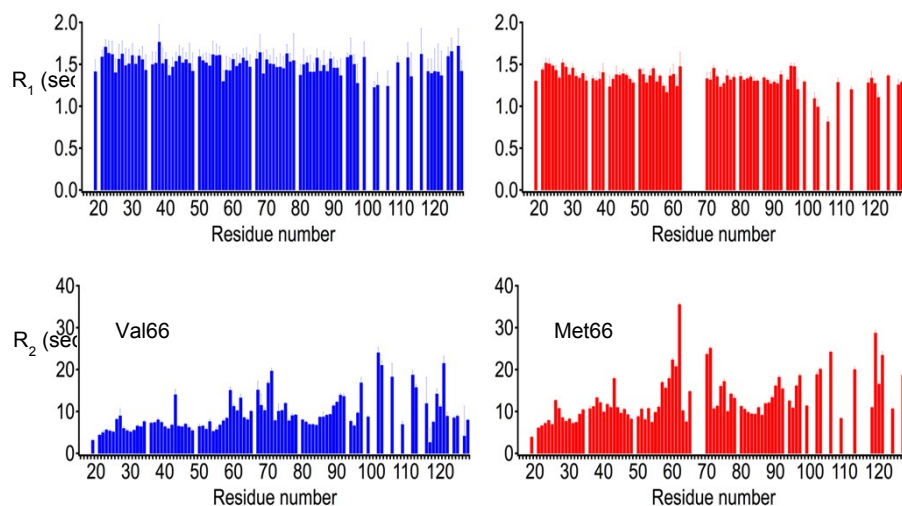
Supplemental Figure 2. Zn²⁺ Induced CD changes.

A, B. CD data were collected using 30 μM prodomain in the apo state (solid line) and in zinc bound state (dashed line) upon addition and preequilibration with 60 μM of Zn²⁺. **A**, CD ellipticity change for 30 μM Val prodomain and right panel displays the **B**, Met prodomain (red). For both Val66 and Met66 prodomains, structural analysis results were derived using K2D2¹



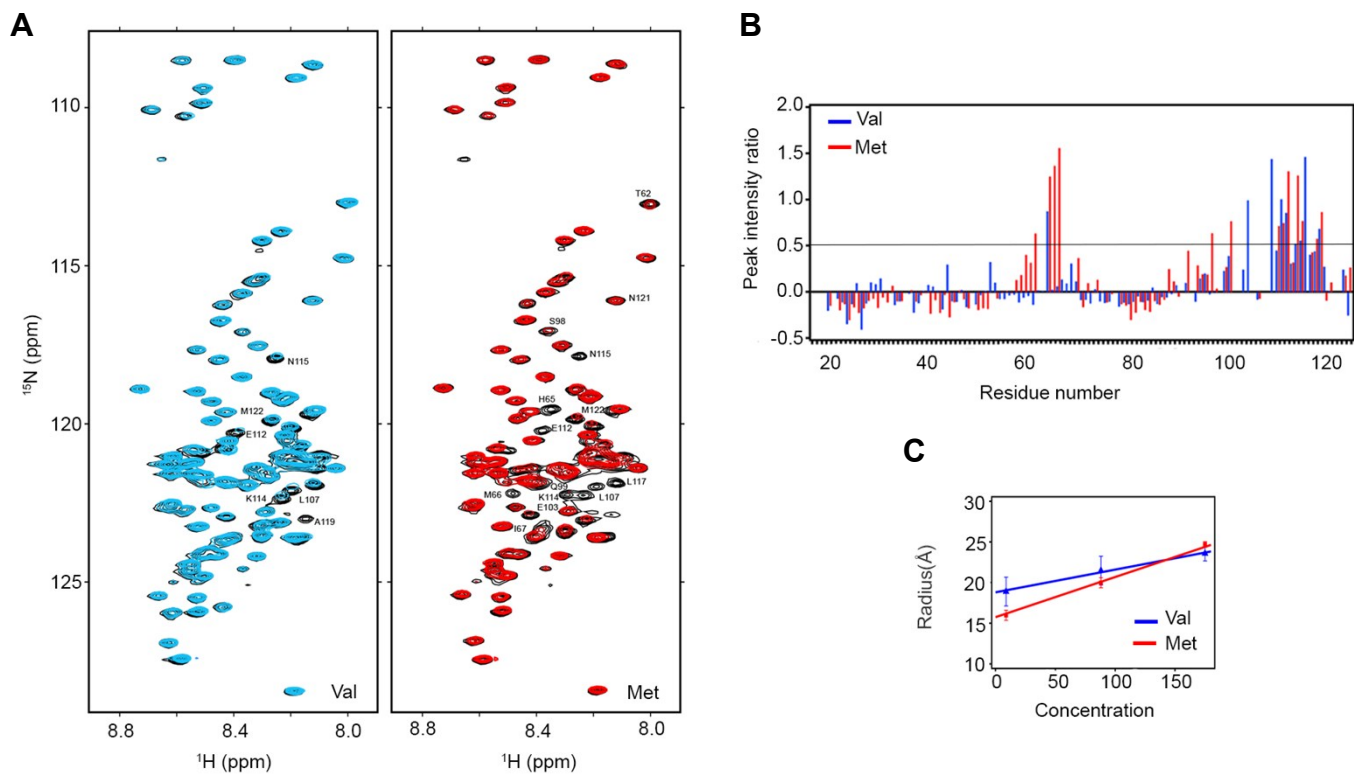
Supplemental Figure 3. Zn²⁺ Binding analysis of Val and Met prodomains.

Upon addition of 1mM CaCl₂ and 1mM MgCl₂ **A**, No UV turbidity changes are observed for both Val and Met prodomain at 10 mM concentration in the presence of both 1mM Ca²⁺ and 1mM Mg²⁺. **B**, Addition of 100 μM zinc, to prodomain solutions containing 1mM Ca²⁺ and 1 mM Mg²⁺, results in development of UV turbidity, indicating that prodomain turbidity changes are specific to addition of Zn²⁺. **C,D**, Low concentrations of prodomain in the presence of zinc produces temporal changes in turbidity development in the presence of **C**, Val and **D**, Met. Prodomain association with zinc displays sigmoidal kinetic behavior indicating multistate initiation, growth kinetics. Met displays enhanced initiation kinetics at lower prodomain concentrations. **E,F** Congo red assay of Zn²⁺ Val and Met prodomain aggregates, respectively. No evident red-shifts or significant absorbance changes are observed, indicating that the solutions lack characteristic changes observed in amyloid fibril formation. **G**, The H40K substitution blocks Zn²⁺ mediated particle formation in both Val and Met prodomain.



Supplemental Figure 4. NMR relaxation measurements detect dynamic mobility differences in Met and Val prodomains in the absence of Zn^{2+} .

NMR ^{15}N longitudinal T_1 and transverse T_2 relaxation measurements were collected as described in prior publications ^{2,3}. NMR relaxation decay curves were fitted to single exponential decay models to extract R_1 and R_2 relaxation rates using python scripts incorporated in NMRFAM-Sparky. Regions of exchange are evident in both isoforms, the extent of chemical regions undergoing exchange are greatly enhanced in Met66, specifically residues 60-72 (66-region) and residues 100-121 (111-region). NMR resonances neighboring Val66 displayed reduced intensity yet were observable, whereas key residues neighboring Met66 are entirely absent (Figure 1E,F, Figure S2A,B). Notably, both isoforms retained full peak intensity in the NMR resonances outside these regions, namely, at the N-terminus (residues 19-58) and intervening residues between the 66-region and 111-regions (residues 74-90) (Figure. S4A,B,D), indicating that these residues do not participate in intermolecular-association in the apo state. This indicates that Met66 substitution significantly increases the propensity for prodomain self-association in comparison to the Val66 isoform.



Supplemental Figure 5. Concentration dependent spectral changes in differ between Val and Met prodomain, in the critical 66-region and C-terminal regions. A ten-fold change in protein concentration reveals differences in **(A)** ^1H - ^{15}N NMR HSQC correlation overlaid spectra showing the backbone amide resonances of 88 μM of Val66/Met (black) and the 8.8 μM of Val (blue), Met (red). **(B)** Changes in relative NMR peak intensity ratios of $I_{88\mu\text{M}}/I_{8.8\mu\text{M}}$ indicate greater losses for Met (red) in the 66 region compared to Val (blue). **(C)** Diffusion measurements indicate concentration dependent increase in hydrodynamic volume for both Val (blue) and Met (red). Conditions under which diffusion rates are unchanged for internal diffusion reference standard DSS and Dioxin. Both NMR peak intensity changes and diffusion measurements indicate Met displays greater concentration dependent intermolecular association consistent with an apparent increase in molecule weight going from 8.8 μM , 88 μM and 157 μM concentrations, indicating a significantly greater intermolecular association than Val.

Supplementary Table 1. Thermodynamic parameters, determined by ITC, for the association of prodomains Val and Met with zinc.

A

	n	Kd(μ M)	Δ G (kJ/mol)	Δ H (kJ/mol)	Δ S (J/mol-K)	-T Δ S (kJ/mol)
Val66	1.5 \pm 0.3	12.5 \pm 1.7	-26.6	16.6 \pm 0.04	153	-43.2
Met66	0.9 \pm 0.1	23.8 \pm 8.4	-25.2	18.9 \pm 0.5	155	-44.0

B

	n1	n2	Kd ₁ (μ M)	Kd ₂ (μ M)	Δ S1 (J/mol-K)	Δ S2 (J/mol-K)	Δ H1 (kJ/mol)	Δ H2 (kJ/mol)
VH40K	1.1 \pm 0.3	1.2 \pm 0.7	3.9 \pm 5.6	347 \pm 566	142	182	1.3 \pm 1.3	29 \pm 36
MH40K	0.5 \pm 0.1	0.6 \pm 0.2	0.4 \pm 0.2	41 \pm 36	131	266	1.9 \pm 0.3	51 \pm 64

The fitted results of the ITC titration data resulting from fitting from titration of 1ul aliquots of 1mM Zn²⁺ into **(A)** 30 μ M Val or Met prodomain solutions or **(B)** 30 μ M Val-H40K (VH40K) or Met-H40K (MH40K) isoform mutants. All data were collected at 10 C. The calculated thermodynamics parameters are the result of separate 3 titration measurements.

Supplemental References:

1. C. Perez-Iratxeta and M. A. Andrade-Navarro, K2D2: estimation of protein secondary structure from circular dichroism spectra, *BMC Struct. Biol.*, 2008, **8**, 25.
2. W. Cao, C. Bracken, N. R. Kallenbach and M. Lu, Helix formation and the unfolded state of a 52-residue helical protein, *Protein science : a publication of the Protein Society*, 2004, **13**, 177-189.
3. Q. Qiao, C. Yang, C. Zheng, L. Fontán, L. David, X. Yu, C. Bracken, M. Rosen, A. Melnick, E. H. Egelman and H. Wu, Structural architecture of the CARMA1/Bcl10/MALT1 signalosome: nucleation-induced filamentous assembly, *Mol. Cell*, 2013, **51**, 766-779.